

A 3-Bit Fully Inkjet-Printed Flexible Chipless RFID for Wireless Concentration Measurements of Liquid Solutions

Zonghao Li, Sharmistha Bhadra

Department of Electrical and Computer Engineering, McGill University, Montreal, QC, H3A 0E9, Canada

Abstract

A fully inkjet-printed flexible chipless RFID tag is presented in this paper. It is based on a coplanar waveguide (CPW) coupled to a multiresonator circuit to encode the information in the frequency domain. Two cross-polarized ultra-wideband (UWB) antennas connected to the CPW receive and transmit the signals. As a proof-of-concept, three spiral resonators are used to encode a 3-bit signature, which can be easily expanded to more bits by adding more resonators. The RFID tag is applied for wireless concentration measurements of liquid solutions by characterizing the insertion loss response. Water/sodium chloride (NaCl) solution and water/isopropanol solution are measured wirelessly by the sensor. A capillary tube is placed on one of the resonators to allow the interaction between the sensor and the solutions. By the observations of measurements, different parameters are used to quantify the sensitivity. The change of the insertion loss at the resonant frequency $|\Delta S_{21}|$ and the half-power 3-dB bandwidth, ΔBW are used to analyze the water/NaCl solution. $|\Delta S_{21}|$ and the shift of resonant frequency, $|\Delta f_{res}|$ are used to analyze the water/isopropanol sample. The proposed RFID shows the potential for measuring liquid solutions wirelessly.

Keywords: Chipless RFID, Concentration sensors, Co-planar waveguide (CPW), Flexible electronics, Liquid solutions, Microwave sensors, Printed electronics, Ultra-wideband (UWB).

¹ 1. Introduction

² Microwave techniques for sensing liquid solutions have been studied nu-

3 merously for applications such as food, beverage, medicine manufacturing,
4 biomedical research, and even oil industry due to their prompt and accurate
5 response, fine accuracy, non-invasive and non-destructive natures [1–4]. Pri-
6 marily, the microwave resonant-type sensors are dominant in the sensing of
7 liquid compounds. The variation of the concentration produces a change of
8 the resonant frequency and quality factor (Q-factor) of a resonator, which
9 provides an easy approach to analyze the liquid solutions.

10 Several liquid compound sensors based on the microwave resonators have
11 been reported in various literature. The rectangular-waveguide resonator de-
12 signed in [4] using TE_{101} mode has achieved a very high sensitivity for both
13 water/NaCl and water-sucrose binary solutions. However, the structure of
14 the rectangular waveguide is bulky and its fabrication method is not suit-
15 able for mass production. The cylindrical resonator using TE_{010} mode has
16 been studied in [5]. It relies on the return loss response to measure the con-
17 centrations for different binary liquid solutions. Planar microwave resonator
18 structure is another popular choice for liquid sensing. In [6], a microstrip
19 line coupled with a complementary split-ring resonator (CSRR) is employed
20 to sense the water-ethanol solution with different concentrations. The so-
21 lutions are passed through the polydimethylsiloxane (PDMS) microfluidic
22 channel on one edge of the CSRR, and the flow will directly contact the res-
23 onator. In [7] the testing liquid sample has to be placed in a cavity on the
24 resonator. This makes the system inappropriate for monitoring continuous
25 liquid flow, and the inevitable residual liquid within the cavity causes drift
26 error. Other planar structure sensors are reported in [8, 9], where the sen-
27 sor microfabrication in the former leads to a higher cost in the prototyping
28 process. To our knowledge, only the liquid sensor in [10] has been reported
29 to be fully printed and flexible. Nevertheless, all above-mentioned sensors
30 require a wired connection to a data readout unit, making them unsuitable
31 for embedded applications. Some designs utilize active components to fur-
32 ther improve the accuracy and sensitivity of the sensors. In [11] an active
33 feedback loop with an amplifier is employed to enhance the Q-factor of the
34 sensor, and a voltage-controlled oscillator with a very high Q-factor is used to
35 analyze organic liquids by monitoring the shift of resonant frequency in [12].
36 Active sensors demonstrate better accuracy and sensitivity. However, the
37 requirement of power supply leads to the necessity of battery replacement,
38 which is not ideal for the long-term and embedded monitoring.

39 Chipless RFID is a contactless communication technology that has no
40 discrete integrated circuit components on the RFID tag. Operating through

41 the energy harvesting of RF signals, it has the advantages of low-cost, high
42 durability, and compatibility with flexible substrates and printing technologies.
43 The research on chipless RFID has progressed marvelously, and chipless
44 RFIDs have been applied to many applications such as item tracking and
45 wireless sensing. So far the only commercial chipless RFID system available
46 is based on the surface acoustic wave (SAW) [13] that encodes the information
47 in the time domain. Frequency domain solutions such as [14, 15] are based
48 on the radar cross section (RCS), and [16, 17] are based on the insertion loss
49 response by the use of microwave multiresonator circuit. Compared to RCS
50 based RFID tags, insertion loss based ones are believed to have less mutual
51 coupling effects, more possible bit numbers, and easier information encoding
52 methods [16]. Between two different approaches of the frequency domain
53 solutions, only RCS based ones have been reported to be fully printed and
54 flexible [15, 18–21]. Although an insertion loss response based rigid-flexible
55 chipless RFID tag is reported in [17], it is manufactured on a laminated board
56 using the traditional printed circuit board (PCB) fabrication method. Some
57 flexible printed microwave multiresonator circuits are reported in [22, 23] to
58 create insertion loss signatures, but they are not able to operate wirelessly.

59 **A fully passive low-cost and wireless sensor is an ideal solution**
60 **to many issues discussed above for microwave liquid sensing.** In
61 **this work, we present a fully inkjet-printed flexible chipless RFID**
62 **tag based on the insertion loss response for concentration measure-**
63 **ment of liquid solution.** It has two major novelties. First, the tag is
64 **fabricated by the inkjet-printing technology.** Unlike conventional
65 **PCB fabrications, the inkjet-printing technology is an additive pro-**
66 **cess, which only deposits material on wanted areas.** Therefore, it
67 **saves more material and lowers the cost.** Second, due to the ab-
68 **sence of solid-state electronics, the tag can be fully inkjet-printed**
69 **on the flexible substrate, making it easier to be attached to various**
70 **shape of items.**

71 The RFID tag consists of a CPW coupled to three spiral resonators that
72 encode the 3-bit information in the frequency spectrum. Two cross-polarized
73 CPW ultra-wideband (UWB) antennas are connected to the CPW to receive
74 and transmit the signals, respectively. The flexible substrate is a $127\ \mu\text{m}$ thick
75 Dupont Kapton polyimide (PI) with excellent electrical properties ($\epsilon_r = 3.4$
76 and $\tan\delta = 0.002$). The flexible conductive ink ($\sigma = 1 \times 10^6\ \text{S/m}$) as well
77 as the inkjet printer are from Voltera. The printer supports up to $250\ \mu\text{m}$
78 feature size and $50\ \mu\text{m}$ deposition thickness. In this work, all simulations

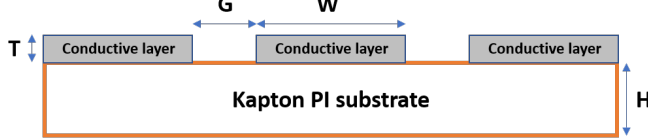


Figure 1: CPW cross section view, where $T = 50 \mu\text{m}$, $H = 127 \mu\text{m}$, $W = 5 \text{ mm}$, and $G = 0.3 \text{ mm}$.

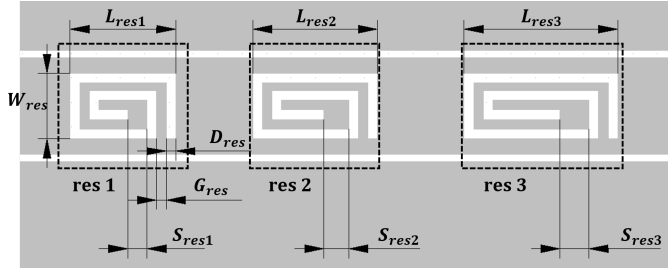


Figure 2: Spiral resonator design, where the grey area is the conductive layer. All resonators ("res 1", "res 2" and "res 3") are centered within the CPW. $L_{res1} = 5.5$, $L_{res2} = 6.5$, $L_{res3} = 8$, $S_{res1} = 1$, $S_{res2} = 1.3$, $S_{res3} = 1.5$, $W_{res} = 3.4$, and $D_{res} = G_{res} = 0.5$, all in millimeter, and the last three parameters are the same for all resonators. From left to right, the resonators are simulated to resonate at 5.1, 4.4 and 3.5 GHz, respectively.

79 are done using ANSYS HFSS, and S -parameters are measured by the vector
 80 network analyzer (VNA, Keysight E5063A). The tag is totally passive. Thus
 81 it is ideal for long-term monitoring. The antennas on the tag enable wireless
 82 measurement, making the tag suitable for the embedded applications.

83 This paper is organized as follow: Section 2 discusses the design of the
 84 chipless RFID system; Section 3 shows the wireless performance of the RFID
 85 tag; Section 4 demonstrates application of the tag for the wireless concen-
 86 tration measurements of water/NaCl and water/isopropanol solutions, and
 87 Section 5 concludes this paper.

88 2. Design of Chipless RFID System

89 2.1. Multiresonator Design

90 To achieve a 50Ω characteristic impedance system, a flexible printed
 91 microstrip line will have an impractical and non-achievable resolution re-
 92 quirement for the printer [24], which motivates us to use the CPW structure.

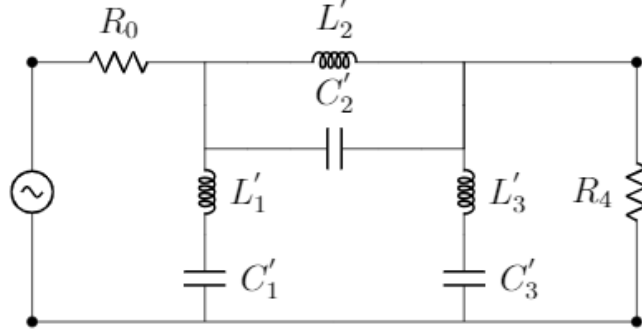


Figure 3: Equivalent lossless circuit model of the CPW coupled to the three resonators, where $R_0 = R_4 = 50 \Omega$, $L'_1 = 132 \text{ nH}$, $C'_1 = 15.3 \text{ fF}$, $L'_2 = 89.8 \text{ pH}$, $C'_2 = 14.43 \text{ pF}$, $L'_3 = 113.7 \text{ nH}$, and $C'_3 = 8.7 \text{ fF}$.

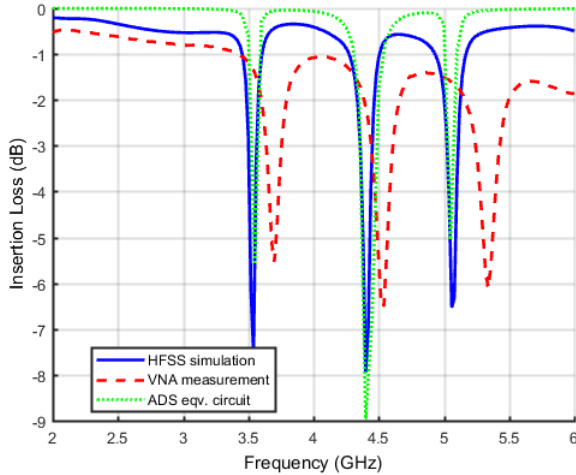


Figure 4: Insertion loss of the CPW coupled to the three resonators, obtained from the HFSS simulation, VNA measurement, and ADS simulation of the equivalent circuit.

Fig. 1 shows the cross-section view of the CPW transmission line used in our design.

The idea of encoding the information in the insertion loss response is to use multiple resonators coupled to the CPW. Fig. 2 shows the layout of the resonator design, where three spiral resonators locate within the CPW transmission line to create a 3-bit spectrum signature. Advanced Design Studio

99 (ADS) is used to extract its equivalent circuit model from the HFSS simu-
 100 lation result based on the Chebyshev low pass filter prototype [25], shown
 101 in Fig. 3. The insertion loss of the equivalent circuit model is plotted to-
 102 gether with the HFSS simulation result and VNA measurement of the printed
 103 prototype design in Fig. 4.

104 The resonances of the equivalent circuit can be calculated by

$$\omega_n = \frac{1}{\sqrt{L'_n C'_n}} \quad \text{and} \quad n = 1, 2, 3. \quad (1)$$

105 Depending on the topology (series and shunt) of the inductor and capacitor,
 106 the Q-factor of each resonance is [26]

$$\begin{cases} Q_{series} = R_0 \sqrt{\frac{C'_n}{L'_n}} & \text{for } n = 1, 3. \\ Q_{shunt} = R_0 \sqrt{\frac{L'_n}{C'_n}} & \text{for } n = 2. \end{cases} \quad (2)$$

107 where

$$\begin{cases} L'_n = \frac{R_0}{\omega_n \Delta C_n} \quad \text{and} \quad C'_n = \frac{\Delta C_n}{\omega_n R_0} & \text{for } n = 1, 3. \\ L'_n = \frac{\Delta L_n R_0}{\omega_n} \quad \text{and} \quad C'_n = \frac{1}{\omega_n \Delta L_n R_0} & \text{for } n = 2. \end{cases} \quad (3)$$

108 For a 50Ω system, $R_0 = R_4 = 50 \Omega$; ω_n is the resonant frequency created by
 109 each corresponding LC circuit; Δ is the fractional bandwidth of the stopband;
 110 and the values for L_n and C_n are the Chebyshev coefficients that can be found
 111 in [27].

112 It can be seen that three plots in Fig. 4 are matching to each
 113 other properly, with some degree of deviations. The insertion loss
 114 of the equivalent circuit is very close to the HFSS simulation result,
 115 with generally higher Q-factors in the resonances as the loss is
 116 neglected in the equivalent circuit model in Fig. 3 for the purpose
 117 of simplicity. The VNA measurement result deviates from the
 118 rest two plots, with an about 200 MHz shift towards the higher
 119 frequency for each resonance. This is due to the imperfect printing

process. When the ink is deposited on the substrate, it tends to spread to the blank area. Therefore, the D_{res} from Fig. 2 will appear smaller on the printed tag than the designed value, leading to a resonance occurs at a slightly higher frequency. Three notches around 3.6, 4.5 and 5.3 GHz have been observed from the measurement that is generated by "res 3", "res 2" and "res 1", respectively. The resonant frequency increases with the dimension shrinkage of the resonator. Three resonances render a 3-bit spectrum signature.

The flexible multiresonator circuit also shows promising insertion loss responses in the bending test. The circuit has been bent along two directions: along the length and width. The testing results can be found in the Appendix A.

2.2. UWB Antenna Design

The encoded frequency signature in Fig. 4 occupies a large bandwidth that requires a UWB antenna to transmit the signal with a low loss. It is also desirable to have an omnidirectional antenna so that the reader antennas can more easily receive the signal from the tag. Therefore, the monopole UWB antenna is preferable on the tag. Flexible printed monopole CPW UWB antennas have been studied in [24]. It is shown that the ellipse-shaped planar structure has a better return loss response. Fig. 5 presents the layout of the inkjet-printed flexible UWB antenna design. The simulated and measured return loss of the antenna is shown in Fig. 6. Both plots are below the -10 dB rule of thumb across the bandwidth of interest. A simulated return loss notch is found around 2 GHz that is outside the bandwidth of interests and therefore not shown. Thus, the deviation is majorly a frequency shift caused by similar reasons happen in the CPW transmission line design. Fig. 7 shows the simulated far-field radiation patterns of the UWB antenna at the central frequency 4 GHz, in both YZ and XZ planes. The UWB antenna demonstrates unidirectional radiation patterns in both planes, with a reasonable polarization purity.

The flexible UWB antenna also shows promising return loss responses in the bending test. The antenna is bent along two directions: along Z -axis and X -axis. The testing results can be found in the Appendix A.

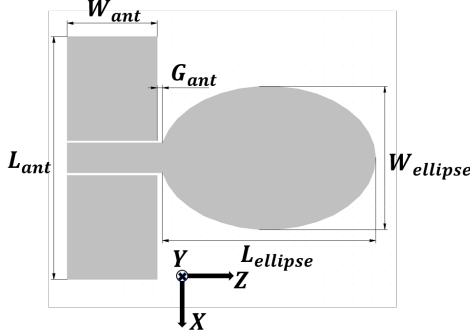


Figure 5: Ellipse UWB antenna design with $W_{ellipse} = 24$, $L_{ellipse} = 35.6$, $G_{ant} = 0.5$, $W_{ant} = 15$, and $L_{ant} = 40.6$, all in millimeter.

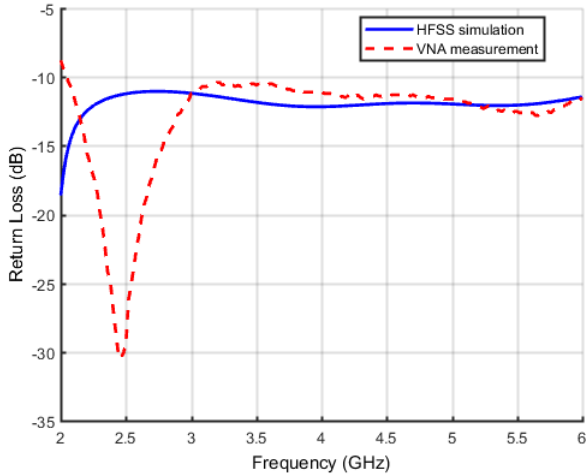


Figure 6: Simulated and measured return loss of the UWB antenna.

154 2.3. *Vivaldi Antenna Design*

155 It is beneficial to choose directional high gain antennas for the reader
 156 so that it can interrogate the RFID tag at a proper distance. A very wide
 157 antenna bandwidth is another requirement as the encoded information oc-
 158 cupies a fairly large interval in the frequency domain, as can be seen in Fig.
 159 4. In this design, we select the Vivaldi antenna due to its high directional
 160 gain, wide bandwidth, and fabrication simplicity. Fig. 8 shows the top and
 161 bottom view of the antenna. We followed the proposed tapered slot antenna
 162 design methodology in [28]. For a Vivaldi antenna, its size and desired band-

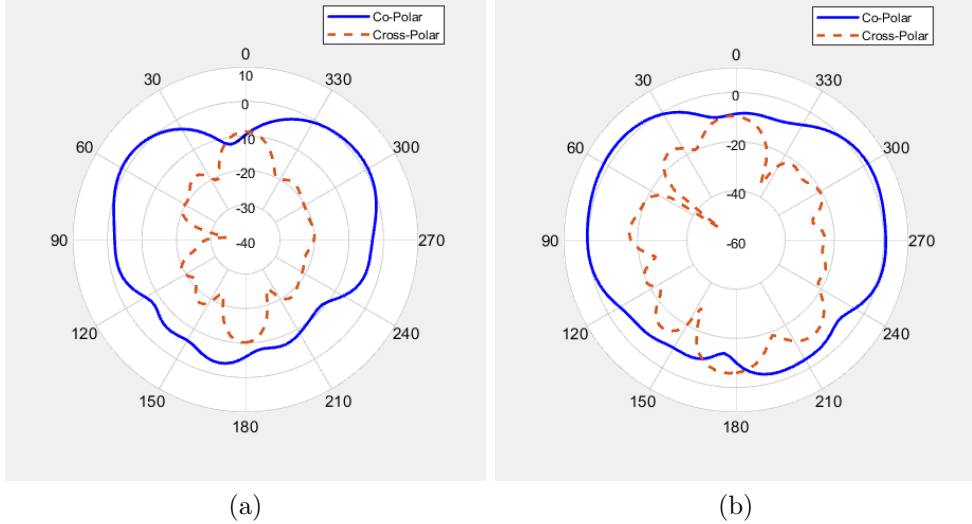


Figure 7: Measured co-polar and cross-polar far-field radiation patterns of the UWB antenna at 4 GHz in the (a) XZ and (b) YZ plane.

width are correlated to the formula of the exponential taper, characterized by the Chebyshev multi-section matching transformer. With a bandwidth requirement of 4 GHz from 2-6 GHz and a 110 mm \times 80 mm dimension specification, the exponential curve is optimized as

$$y = 0.4913e^{0.0425x} - 0.0413 \quad (4)$$

The antenna substrate board is Rogers 3206 with $\epsilon_r = 6.15$ and thickness $t = 1.27\text{mm}$. The bottom plane, where the microstrip-to-slotline transition is located, consists of three different impedance transformers (L_1 , $L_2 - L_3$, and L_4) and a 90-degree radial stub so that a minimum loss and the desired bandwidth can be achieved [29]. Fig. 9 shows the measured co-planar and cross-polar radiation patterns of the designed Vivaldi antenna at 4 GHz. A near 30-dB gain difference has been achieved in the Z direction, allowing a good polarization purity and directivity. Fig. 10 shows the return loss and gain of the antenna along the Z direction across the interested bandwidth. A more than 6 dB average gain and a return loss smaller than -10 dB have been achieved from 2 - 6 GHz.

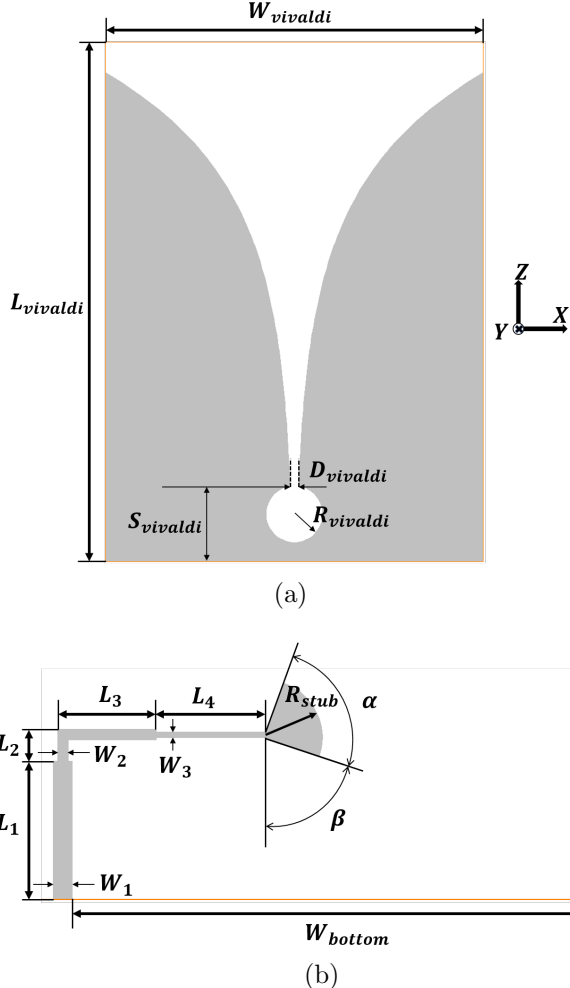


Figure 8: (a) Top plane of the Vivaldi antenna, where $W_{vivaldi} = 80$, $L_{vivaldi} = 110$, $S_{vivaldi} = 16$, $D_{vivaldi} = 1.85$, and $R_{vivaldi} = 3$. (b) bottom plane of the antenna, where $W_{bottom} = 58.52$ is the distance from the microstrip line to the right edge of the board, $L_1 = 14$, $L_2 = 3.24$, $L_3 = 10$, $L_4 = 11.2$, $W_1 = 1.88$, $W_2 = 1.08$, $W_3 = 0.31$, $R_{stub} = 6.33$, $\alpha = 90^\circ$, and $\beta = 70^\circ$. All length dimension are in millimeter.

¹⁷⁸ **3. Flexible Printed Chipless RFID Tag**

¹⁷⁹ The proposed chipless RFID tag is shown in Fig. 11. It is noted that,
¹⁸⁰ to integrate two UWB antennas in a cross-polarized fashion on the tag, the

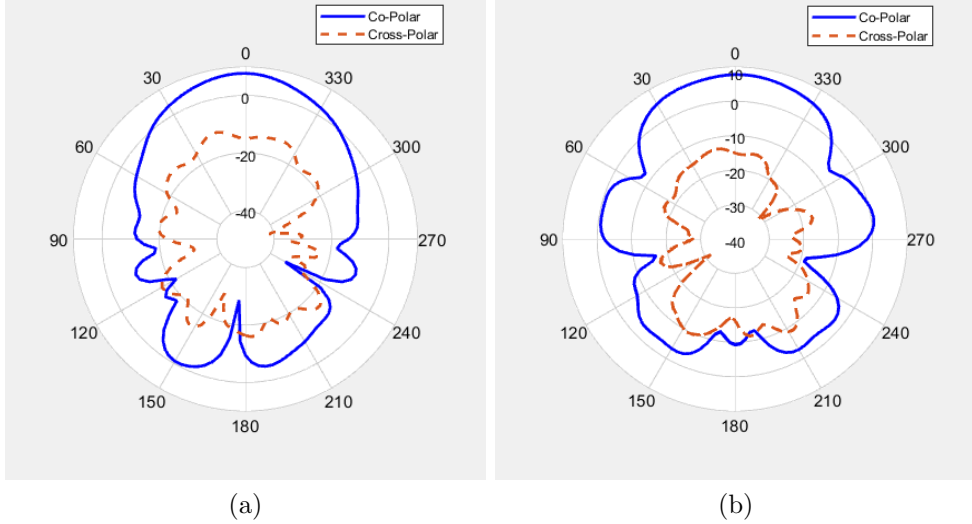


Figure 9: Measured co-polar and cross-polar far-field radiation patterns of the Vivaldi antenna at 4 GHz in the (a) XZ and (b) YZ plane.

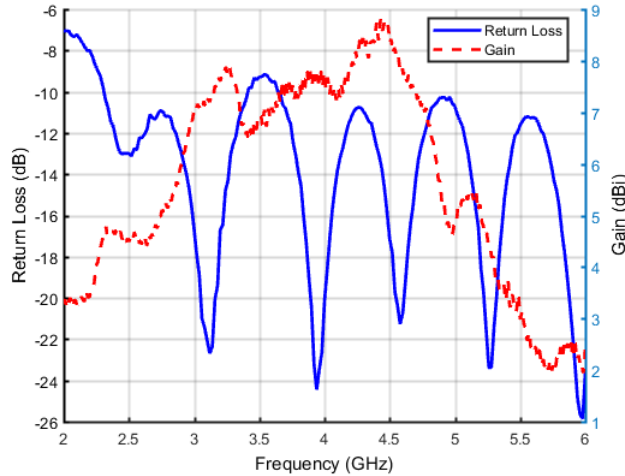


Figure 10: Measured return loss and gain of Vivaldi reader antenna.

181 CPW bend is required. A common but not optimized method is the right-
 182 angle bend used in [17]. However, unlike the regular copper cladding, the
 183 lossy conductive ink and the thick conductive layer lead to a major loss in our
 184 simulations with this structure. This is primarily caused by the slotline mode

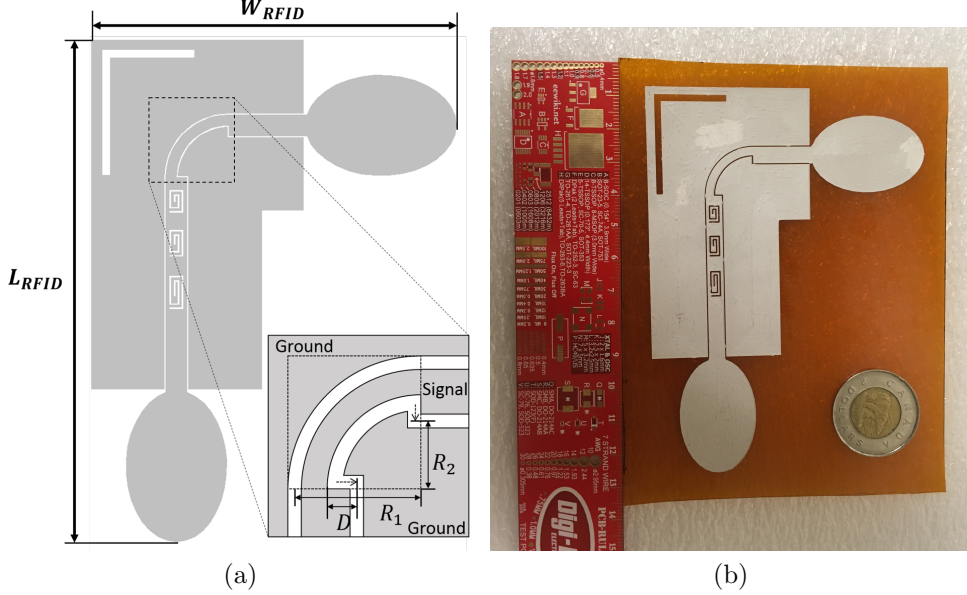


Figure 11: (a) Geometry of the RFID tag with $W_{RFID} = 87.1$, $L_{RFID} = 119.7$. The 90° circular bend with the slow-wave compensation structure is highlighted in the dashline box, with $D = 2.65$, $R_1 = 9.615$, and $R_2 = 15.15$, all parameters are in millimeter. The dimension of the CPW, the multiresonator circuit, and the UWB antennas are the same as the ones in Section 2.1 and 2.2. (b) The inkjet-printed flexible chipless RFID tag.

185 excitations within the CPW bend due to the unequal traveling distances of
 186 the waves. To mitigate this issue, we apply the 90° circular bend with a novel
 187 slow-wave compensation structure [30] in our design to decrease the losses,
 188 presented in Fig. 11 (a). This does not need extra components and materials
 189 like other compensation methods such as wire-bond techniques or dielectric
 190 overlay techniques.

191 The printed tag is shown in Fig. 11 (b). The size of the tag
 192 is not optimally compact but is adequate for some applications,
 193 such as logistic tracking and freshness sensing in food packages.
 194 To further shrink down the size of the tag, one can decrease the
 195 size of the resonators and UWB antennas to shift the bandwidth
 196 of the tag to the upper-frequency range. Additionally, one can
 197 decrease the area of the ground plane to an optimal size that does
 198 not change the resonances the tag.

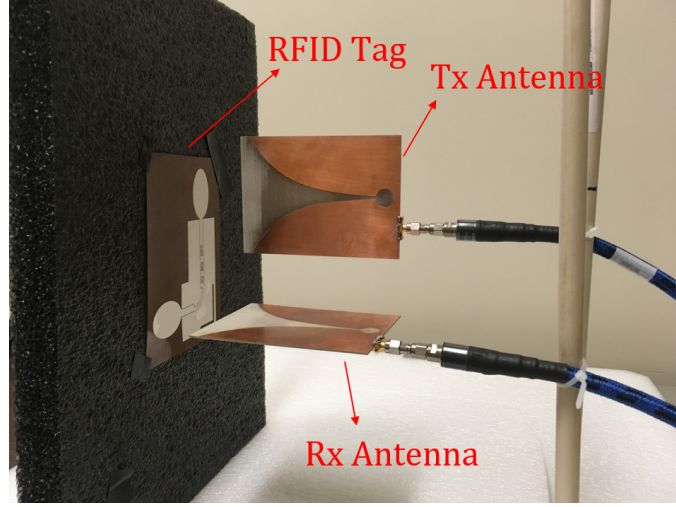


Figure 12: Wireless experiment setup for the chipless RFID tag at 5 cm.

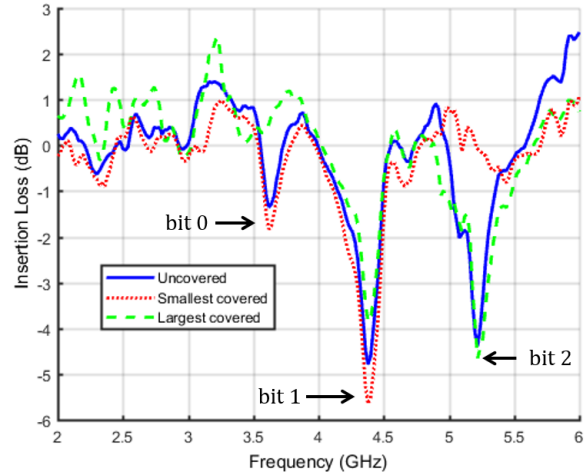


Figure 13: Insertion loss response of the tag at 5 cm in distance to the Tx and Rx antennas in the ambient environment, with and without resonators covered.

199 The chipless RFID tag is tested in the ambient environment. Fig. 12
 200 shows the testing setup. Two cross-polarized Vivaldi antennas are used to
 201 transmit and receive the signals from the tag that is distanced 5 cm away.
 202 The wireless measurement results of the whole tag are presented in Fig. 13.
 203 All plots are generated after subtracting the insertion loss response of the ref-

204 reference tag that is printed out separately without any resonators. Therefore,
205 the net responses are mostly contributed by the resonators. Resonators "res
206 3", "res 2" and "res 1" excite three notches around 3.6, 4.4, and 5.3 GHz,
207 respectively, which are encoded as "bit 0", "bit 1" and "bit 2". To further
208 verify the correspondences between resonators and notches, a copper tape is
209 used to cover one resonator at a time. Initially, all resonators are uncovered,
210 followed by covering the resonator "res 1", and then resonator "res 3". When
211 "res 1" is covered (shorted), the resonance at 5.3 GHz disappears, whereas
212 the rest two resonances remain at their frequencies. The same phenomena
213 is observed with "res 3" covered: the resonance at 3.6 GHz vanishes while
214 the rest two retain. With this idea, one has the freedom of encoding differ-
215 ent 3-bit messages based on the appearance of notches. It should be noted
216 that the net insertion responses of the resonators are above 0 dB at some
217 frequencies, which is due to the imperfect subtraction from the reference tag
218 that does not physically contribute to any gain.

219 It is worth mentioning that since the tag is characterized in the ambi-
220 ent environment, and its conductive layer is lossier than the regular copper
221 cladding used in commercial microwave circuit boards, we believe that it
222 would demonstrate a longer reading range and a higher Q-factor with the
223 resonances in the anechoic chamber if it is fabricated with a more conductive
224 ink. Compared to the RFID systems proposed in [16], our design in the am-
225 bient environment has demonstrated an adequate ability for the information
226 recognition in the same distance.

227 4. Wireless Concentration Measurements of Liquid Solutions

228 For the proof-of-concept, two different liquid solutions are prepared for the
229 wireless concentration measurement, the water/NaCl and water/isopropanol
230 solutions. The NaCl concentration is varied in the range [0, 100] $\mu\text{g}/\text{ml}$
231 with an increment of 10 $\mu\text{g}/\text{ml}$ per sample. The isopropanol concentration
232 is varied in the range of [0, 99] vol% in terms of volume fraction, with an
233 increment of 20 vol% per sample. Fig. 14 shows the experimental setup for
234 the measurements. Similar to Fig. 12, two cross-polarized Vivaldi antennas
235 interrogate the RFID tag that is placed 5 cm away in the ambient environ-
236 ment. A capillary tube with an inner radius $r_c = 0.75$ mm is centered on the
237 top of the resonator "res 2" to achieve a better sensitivity [5]. The tube is
238 filled and drained with different liquid samples by a syringe, and the data are
239 collected by the VNA. The experiments are operated in room temperature.

240 Primarily, the appearance of the liquid solutions alters the capacitance C'_2
 241 of the resonator "res 2" in Fig. 3. As discussed in [6], C'_2 can be approximated
 242 as

$$C'_2 = C_0 + \epsilon_{solutions} C_{tube} \quad (5)$$

243 where C_0 is the capacitance of the "res 2" excluding the capillary channel, and
 244 C_{tube} is the capacitance contributed by the solution-filled capillary channel.
 245 The complex dielectric constant of the liquid solution is

$$\epsilon_{solutions} = \epsilon'_{solutions} + j\epsilon''_{solutions} \quad (6)$$

246 From equations (1) - (3) and (5) - (6), it can be seen that the Q-factor, as
 247 well as the resonant frequency, are related to the intrinsic dielectric property
 248 of the liquid samples themselves. **It is shown in the same literature that**
 249 $\epsilon'_{solutions}$ **and** $\epsilon''_{solutions}$ **have different contributions on the change of the**
 250 **Q-factor and the resonant frequency, respectively.** Also, for differ-
 251 ent solutions, the increase of the concentration will cause different
 252 degree of change of $\epsilon'_{solutions}$ and $\epsilon''_{solutions}$. Therefore, it is convenient
 253 to use the parameter that varies noticeably as the concentration
 254 of the solution changes. As presented in [4], the water/NaCl so-
 255 lutions produce a dominant change on the Q-factor. Therefore,
 256 to extract the correlation between the concentration variation and
 257 the corresponding insertion loss response, the change of the inser-
 258 tion loss at the resonant frequency $|\Delta S_{21}|$ and the half-power 3-dB
 259 bandwidth ΔBW are analyzed for the water/NaCl samples. On
 260 the other hand, since the water/isopropyl alcohol solutions also
 261 produce a noticeable change on the resonant frequency in addi-
 262 tion to the Q-factor, $|\Delta S_{21}|$ and the shift of the resonant frequency
 263 $|\Delta f_{res}|$ are analyzed for the water/isopropyl alcohol samples. The
 264 definitions of $|\Delta S_{21}|$ and $|\Delta f_{res}|$ are defined mathematically as

$$\begin{cases} |\Delta S_{21}| = |S_{21,liquid} - S_{21,water}| \\ |\Delta f_{res}| = |f_{liquid} - f_{water}| \end{cases} \quad (7)$$

265 where $S_{21,liquid}$ and f_{liquid} represent the insertion loss at the resonant fre-
 266 quency and resonant frequency of different concentration liquid samples, re-
 267 spectively. $S_{21,water}$, and f_{water} are the insertion loss at the resonant frequency
 268 and resonant frequency of pure water.

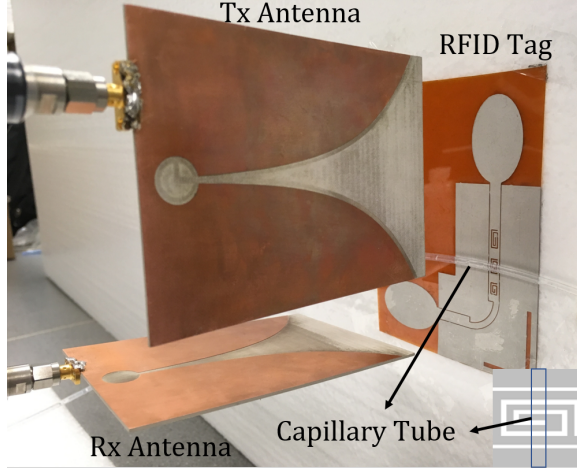


Figure 14: Wireless measurement setup for the solutions with various concentrations. The capillary tube is place on the top the resonator "res 2".

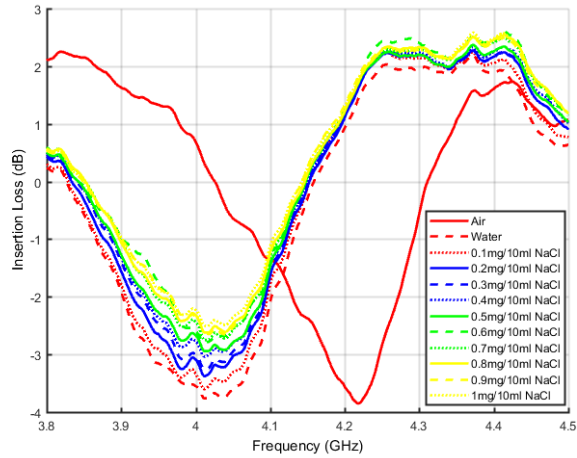


Figure 15: Insertion loss response of the resonator "res 2" versus various water/NaCl solutions with different concentrations in the room temperature.

Fig. 15 shows the insertion loss response of the resonator "res 2" with the water/NaCl samples. It can be noticed that the concentration variation mainly contributes to the change of the Q-factor. $|\Delta S_{21}|$ and ΔBW versus different NaCl concentrations from the frequency response are plotted in Fig. 16 and 17, respectively, together with the second-order polynomial fitting. In

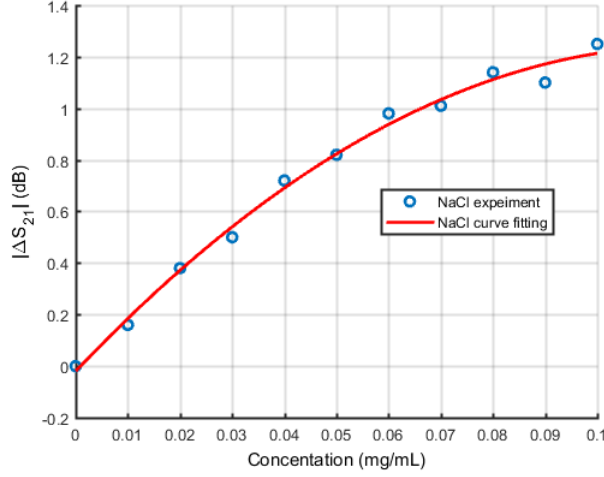


Figure 16: Measured $|\Delta S_{21}|$ variation with NaCl concentrations in the range [0, 100] $\mu\text{g}/\text{ml}$ with an increment of 10 $\mu\text{g}/\text{ml}$ per sample.

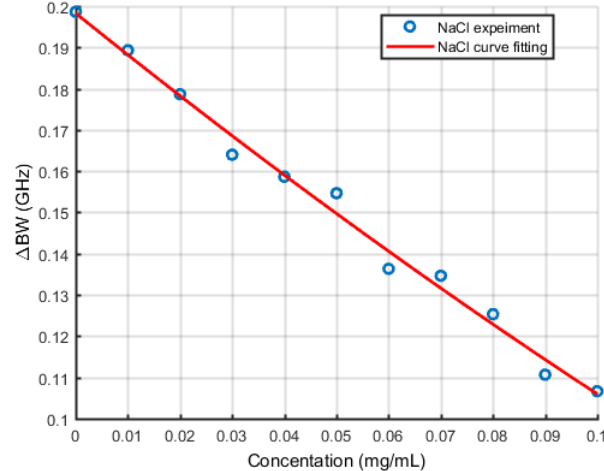


Figure 17: Measured ΔBW variation with NaCl concentrations in the range [0, 100] $\mu\text{g}/\text{ml}$ with an increment of 10 $\mu\text{g}/\text{ml}$ per sample.

274 Fig. 16, the sensor demonstrates a better sensitivity and linearity when the
 275 NaCl concentrations are low. The linearity degrades when the concentration
 276 is above 60 $\mu\text{g}/\text{ml}$. Within [0, 60] $\mu\text{g}/\text{ml}$, $|\Delta S_{21}|$ response has an average
 277 sensitivity of 0.03 dB/($\mu\text{g}/\text{ml}$). It is interesting to note that ΔBW in Fig.

278 17 shows a very good linearity across the whole concentration range, with
 279 an average sensitivity of 1 MHz/(μ g/ml). The shift of resonant frequency
 280 is not noticeable in the wireless measurement. As explained before, the wa-
 281 ter/NaCl solution has a more dominant influence on the Q-factor rather than
 282 the resonant frequency. To magnify the sensitivity for the shift of resonant
 283 frequency, it is advisable to increase the inner diameter of the capillary. The
 284 trade-off, however, would be a higher possibility of introducing air bubbles
 285 in the tube that would destroy the homogeneity of the liquid solutions [4].
 286 Across the whole testing concentration range, the second-order regression
 287 result for $|\Delta S_{21}|$ in Fig. 16 is

$$y = -90.5594x^2 + 21.3923x - 0.0199 \quad (8)$$

288 and for ΔBW in Fig. 17 is

$$y = 0.9596x^2 - 1.0193x + 0.1983 \quad (9)$$

289 Fig. 18 shows the insertion loss response of water/isopropanol samples
 290 measured by the same resonator. Noted that both Q-factor and resonant fre-
 291 quency change noticeably for this solution. It can be seen that the depth of
 292 S_{21} at the resonant frequency decreases with the increase of the isopropanol
 293 concentration. Meanwhile, the resonant frequency also shifts up noticeably.
 294 $|\Delta S_{21}|$ and $|\Delta f_{res}|$ response versus different isopropanol concentrations are
 295 shown in Fig. 19 and 20, respectively, together with the second-order poly-
 296 nomial fitting result. When the isopropanol concentration is low, neither
 297 $|\Delta S_{21}|$ nor $|\Delta f_{res}|$ changes obviously. When the concentration of isopropanol
 298 is above 20 vol%, both $|\Delta S_{21}|$ and $|\Delta f_{res}|$ increase monotonically with the
 299 increase of the concentration. In Fig. 19, $|\Delta S_{21}|$ plot shows a good linearity
 300 within [20, 80] vol% concentration range with a sensitivity of 0.3 dB/(20
 301 vol%). $|\Delta f_{res}|$ plot in Fig. 20 shows a good linearity within [40, 99] vol%
 302 concentration range with an average sensitivity of 30 MHz/(20 vol%). Across
 303 the whole testing concentration range, the second-order regression result for
 304 $|\Delta S_{21}|$ in Fig. 19 is

$$y = 2.0334x^2 - 0.453x + 0.0286 \quad (10)$$

305 and for ΔBW in Fig. 20 is

$$y = 0.0794x^2 + 0.0124x - 0.002 \quad (11)$$

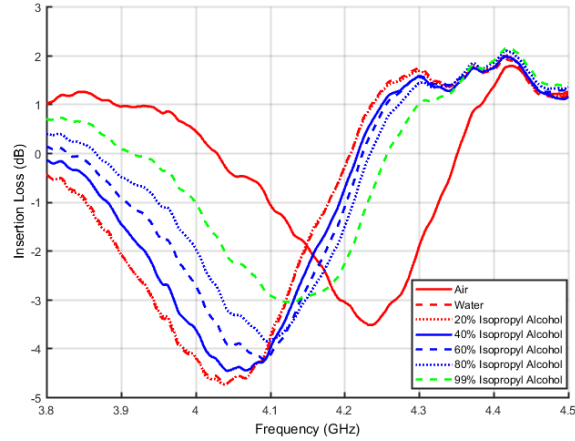


Figure 18: Insertion loss response of the resonator "res 2" versus various water/isopropanol solutions with different concentrations in the room temperature.

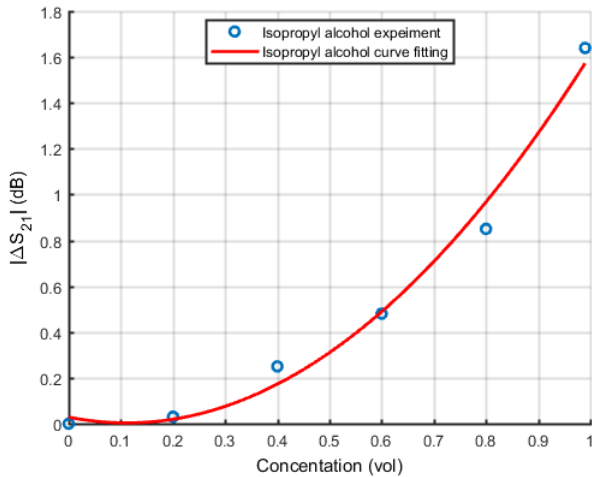


Figure 19: Measured $|\Delta S_{21}|$ variation with isopropyl alcohol concentrations in the range [0, 99] vol% with an increment of 20 vol% per sample.

Table 1 summarizes the performance of the sensor in concentration measurements of liquid solutions. It can be seen that for one kind of liquid solution, different ways of data extraction could lead to different linearity and sensitivity. Therefore, it is suggesting to use the parameter that has a higher sensitivity to measure the concentration. **Table 2 shows the comparison**

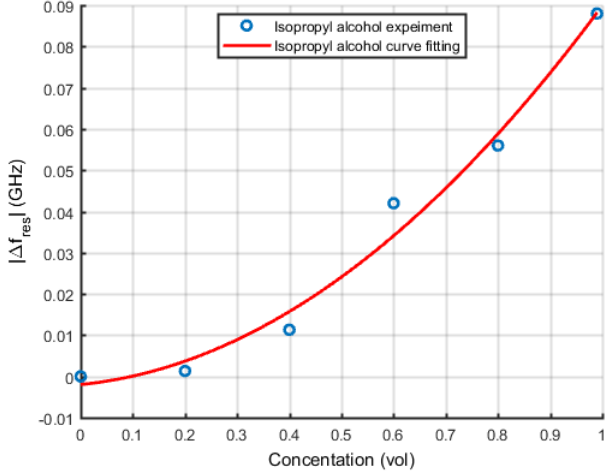


Figure 20: Measured $|\Delta f_{res}|$ variation with isopropanol concentrations in the range [0, 99] vol% with an increment of 20 vol% per sample.

Table 1: Performance summary of the sensor at 5 cm in room temperature

Solution	Concentration Range	Measured Parameters	Linear Range	Sensitivity
water/NaCl	[0, 100] $\mu\text{g}/\text{ml}$	$ \Delta S_{21} $	[0, 60] $\mu\text{g}/\text{ml}$	0.03 dB/ $(\mu\text{g}/\text{ml})$
		ΔBW	[0, 100] $\mu\text{g}/\text{ml}$	1 MHz/ $(\mu\text{g}/\text{ml})$
water/isopropanol	[0, 99] vol%	$ \Delta S_{21} $ $ \Delta f_{res} $	[20, 80] vol% [40, 99] vol%	0.3 dB/(20 vol%) 30 MHz/(20 vol%)

311 **of the proposed design to other microwave liquid concentration
 312 sensors, but with different solution samples.** In general, our sensor
 313 has the advantages of wireless operation, low-cost, and flexibility. It should
 314 be remarked that in contrast to the designs in [4–12], our sensor operates
 315 wirelessly in the ambient environment, and it is strongly subjected to ambi-
 316 ent noises. Therefore, the sensitivity of the sensor is drastically degenerated,
 317 showing a limited linear range for the concentration measurements. The
 318 inevitable air bubbles in the capillary tube also cause the error due to the
 319 inhomogeneity of the liquid, which can be mitigated by using a smaller di-
 320 ameter capillary tube. Nevertheless, it will degrade the evaluation of ΔBW

Table 2: Comparison summary with some microwave liquid concentration sensors

Paper	Wireless	Non-contact	Operating Frequency (GHz)	Fabrication Method	Solutions	Sensitivity
This work	Yes (5 cm)	Yes	3.2 - 3.8	Inkjet-printed Flexible substrate	water/NaCl [0, 100] $\mu\text{g}/\text{ml}$ water/isopropyl alcohol [0, 99] vol%	$ \Delta S_{21} : 0.03 \text{ dB}/(\mu\text{g}/\text{ml})$ $ \Delta BW : 1 \text{ MHz}/(\mu\text{g}/\text{ml})$ $ \Delta S_{21} : 0.3 \text{ dB}/(20 \text{ vol}\%)$ $ \Delta f_{res} : 30 \text{ MHz}/(20 \text{ vol}\%)$
[4]	No	Yes	1.88 - 1.94	Aluminum machining	water/NaCl [0, 10] mg/ml water/sucrose [0, 25] mg/ml	$ \Delta S_{21} : 2 \text{ dB}/(\text{mg}/\text{ml})$ $ \Delta BW : 5 \text{ MHz}/(\text{mg}/\text{ml})$ $ \Delta S_{21} : 0.018 \text{ dB}/(\text{mg}/\text{ml})$ $ \Delta f_{res} : 40 \text{ MHz}/(\text{mg}/\text{ml})$
[5]	No	Yes	1.858 - 1.859	Metal machining	water/NaCl [0, 4] wt%	$ \Delta S_{11} : 0.4 \text{ dB}/(\text{mg}/\text{ml})$
[6]	No	No	1.2 - 2.8	PCB fabrication	water/KMnO ₄ [0, 1.7] wt%	$ \Delta S_{11} : 0.2 \text{ dB}/(\text{mg}/\text{ml})$
[7]	No	No	2 - 3	PCB fabrication	water/sugar [0, 11] wt%	$ \Delta S_{11} : 0.0065 \text{ dB}/(\text{mg}/\text{ml})$
[10]	No	Yes	8 - 12	Inkjet-printed Flexible substrate	water/alcohol [0, 10] vol%	$ \Delta S_{11} : 0.14 \text{ dB}/(\text{mg}/\text{ml})$
					water/ethanol [0, 100] vol%	$ \Delta S_{21} : 0.5 \text{ dB}/(20\% \text{ water})$ $ \Delta f_{res} : 100 \text{ MHz}/(20\% \text{ water})$
					water/sucrose [0, 1] g/ml	$ \Delta S_{21} : 4.95 \text{ dB}/(\text{g}/\text{ml})$
					water/NaCl [0 - 29.2] mg/ml	$ \Delta S_{21} : 0.188 \text{ dB}/(\text{mg}/\text{ml})$ $ \Delta f_{res} : 7.26 \text{ MHz}/(\text{mg}/\text{ml})$

321 [4]. The lossy conductive ink used for the sensor is another factor for de-
322 caying its accuracy. With all these issues addressed, it is still interesting to
323 see that within the linear response region, the sensor has a good sensitivity
324 over a low concentration range of NaCl solutions, in contrast to [4, 5, 10].
325 **Therefore, it is advisable to employ this sensor in the applications**
326 **where low concentration measurement is interested.** Furthermore, to
327 demonstrate its applicability for measuring other liquids, the sensor is used
328 for measuring the isopropanol solutions with different concentrations, gener-
329 ating usable results with a coarse concentration increment. It is reasonable
330 to believe that our sensor will achieve a better sensitivity when it is operated
331 in the wired mode.

332 **5. Conclusion**

333 A fully inkjet-printed flexible chipless RFID is presented in this paper.
334 The tag has a 3-bit information storage capability that encodes the message
335 through the insertion loss response. The tag has been successfully tested
336 in the ambient environment with a 5 cm separation from the reader anten-
337 nas. We further apply it for the wireless concentration measurements of
338 water/NaCl and water/isopropanol solutions to demonstrate its potential in
339 the wireless sensing. The change of the Q-factor with different NaCl concen-
340 trations is the most noticeable observation. Different isopropanol concentra-
341 tions change both the Q-factor and resonant frequency. Promising results
342 have been collected. Unlike other microwave liquid sensing platforms, it is
343 the first reported wireless flexible printed liquid concentration sensor that has
344 the advantages of passive, low-cost, contactless, flexible, and fast prototyping
345 with the possibility of attaching it to a various shape of items.

346 **Acknowledgment**

347 The authors would like to thank Don Pavlasek from McGill University for
348 manufacturing the Vivaldi antennas, and Maxime Thibault from Polytech-
349 nique Montreal for the antenna characterizations. This work is supported by
350 the Natural Sciences and Engineering Research Council of Canada (NSERC)
351 (Grant number: NSERC RGPIN-2017-05176).

352 **References**

- 353 [1] O. Lund Bo, E. Nyfors, Application of microwave spectroscopy for the
354 detection of water fraction and water salinity in water/oil/gas, *Journal*
355 of Non-Crystalline Solids
- 356 [2] M. Kent, D. Anderson, Dielectric studies of added water in poultry meat
357 and scallops, *Journal of Food Engineering* 28 (1996) 239 – 259.
- 358 [3] K. K. Joshi, R. D. Pollard, Microstrip resonator technique for non-
359 destructive moisture/permittivity measurement, in: 1999 IEEE MTT-S
360 International Microwave Symposium Digest (Cat. No.99CH36282), volume 4, pp. 1863–1866 vol.4.
- 362 [4] G. Gennarelli, S. Romeo, M. R. Scarfi, F. Soldovieri, A microwave res-
363 onant sensor for concentration measurements of liquid solutions, *IEEE*
364 *Sensors Journal* 13 (2013) 1857–1864.
- 365 [5] B. Kapilevich, B. Litvak, Microwave sensor for accurate measurements
366 of water solution concentrations, in: 2007 Asia-Pacific Microwave Con-
367 ference, pp. 1–4.
- 368 [6] A. Ebrahimi, W. Withayachumnankul, S. Al-Sarawi, D. Abbott, High-
369 sensitivity metamaterial-inspired sensor for microfluidic dielectric char-
370 acterization, *IEEE Sensors Journal* 14 (2014) 1345–1351.
- 371 [7] S. Harnsoongnoen, A. Wanthon, Coplanar waveguides loaded with a
372 split ring resonator-based microwave sensor for aqueous sucrose solu-
373 tions, *Measurement Science and Technology* 27 (2015) 015103.
- 374 [8] T. Chretiennot, D. Dubuc, K. Grenier, A microwave and microfluidic
375 planar resonator for efficient and accurate complex permittivity char-
376 acterization of aqueous solutions, *IEEE Transactions on Microwave The-*
377 *ory and Techniques* 61 (2013) 972–978.
- 378 [9] A. A. Abduljabar, D. J. Rowe, A. Porch, D. A. Barrow, Novel microwave
379 microfluidic sensor using a microstrip split-ring resonator, *IEEE Trans-*
380 *actions on Microwave Theory and Techniques* 62 (2014) 679–688.
- 381 [10] A. Chahadih, P. Y. Cresson, Z. Hamouda, S. Gu, C. Mismer, T. Lasri,
382 Microwave/microfluidic sensor fabricated on a flexible kapton substrate

- 383 for complex permittivity characterization of liquids, Sensors and Actuators A: Physical 229 (2015) 128 – 135.
- 384
- 385 [11] M. H. Zarifi, M. Rahimi, M. Daneshmand, T. Thundat, Microwave ring
386 resonator-based non-contact interface sensor for oil sands applications,
387 Sensors and Actuators B: Chemical 224 (2016) 632 – 639.
- 388 [12] V. Sekar, W. J. Torke, S. Palermo, K. Entesari, A self-sustained mi-
389 crowave system for dielectric-constant measurement of lossy organic liq-
390 uids, IEEE Transactions on Microwave Theory and Techniques 60 (2012)
391 1444–1455.
- 392 [13] C. S. Hartmann, A global saw id tag with large data capacity, in: 2002
393 IEEE Ultrasonics Symposium, 2002. Proceedings., volume 1, pp. 65–69
394 vol.1.
- 395 [14] F. Costa, S. Genovesi, A. Monorchio, A chipless rfid based on mul-
396 tiresonant high-impedance surfaces, IEEE Transactions on Microwave
397 Theory and Techniques 61 (2013) 146–153.
- 398 [15] M. Borgese, F. A. Dicandia, F. Costa, S. Genovesi, G. Manara, An
399 inkjet printed chipless rfid sensor for wireless humidity monitoring, IEEE
400 Sensors Journal 17 (2017) 4699–4707.
- 401 [16] S. Preradovic, N. C. Karmakar, Design of fully printable planar chipless
402 rfid transponder with 35-bit data capacity, in: Proc. 2009 European
403 Microwave Conference (EuMC), pp. 013–016.
- 404 [17] S. Preradovic, N. C. Karmakar, Multiresonator based chipless rfid tag
405 and dedicated rfid reader, in: 2010 IEEE MTT-S International Mi-
406 crowave Symposium, pp. 1–1.
- 407 [18] R. Nair, M. Barahona, D. Betancourt, G. Schmidt, M. Bellmann,
408 D. Hoft, D. Plettemeier, A. Hubler, F. Ellinger, A fully printed pas-
409 sive chipless rfid tag for low-cost mass production, in: The 8th Eu-
410 ropean Conference on Antennas and Propagation (EuCAP 2014), pp.
411 2950–2954.
- 412 [19] J. G. D. Hester, M. M. Tentzeris, Inkjet-printed flexible mm-wave van-
413 atta reflectarrays: A solution for ultralong-range dense multitag and

- 414 multisensing chipless rfid implementations for iot smart skins, IEEE
415 Transactions on Microwave Theory and Techniques 64 (2016) 4763–4773.
- 416 [20] A. Vena, L. Sydnheimo, L. Ukkonen, M. M. Tentzeris, A fully inkjet-
417 printed chipless rfid gas and temperature sensor on paper, in: 2014
418 IEEE RFID Technology and Applications Conference (RFID-TA), pp.
419 115–120.
- 420 [21] D. Betancourt, K. Haase, A. Hbler, F. Ellinger, Bending and folding
421 effect study of flexible fully printed and late-stage codified octagonal
422 chipless rfid tags, IEEE Transactions on Antennas and Propagation 64
423 (2016) 2815–2823.
- 424 [22] W. Su, , B. Cook, M. Tentzeris, All-inkjet-printed microfluidics-based
425 encodable flexible chipless rfid sensors, in: 2016 IEEE MTT-S Interna-
426 tional Microwave Symposium (IMS), pp. 1–4.
- 427 [23] M. E. Jalil, M. K. A. Rahim, N. A. Samsuri, R. Dewan, Flexible
428 printed chipless rfid tag using metamaterial-split ring resonator, Ap-
429 plied Physics A 122 (2016) 348.
- 430 [24] H. R. Khaleel, H. M. Al-Rizzo, D. G. Rucker, S. Mohan, A compact
431 polyimide-based uwb antenna for flexible electronics, IEEE Antennas
432 and Wireless Propagation Letters 11 (2012) 564–567.
- 433 [25] J.-S. Lim, C.-S. Kim, Y.-T. Lee, D. Ahn, S. Nam, A spiral-shaped
434 defected ground structure for coplanar waveguide, IEEE Microwave
435 and Wireless Components Letters 12 (2002) 330–332.
- 436 [26] D. M. Pozar, Microwave Engineering, John Wiley & Sons, pp. 413–414.
- 437 [27] L. Y. G. L. Matthaei, E. M. T. Jones, Microwave Filters, Impedance-
438 Matching Networks, and Coupling Structures, Artech House.
- 439 [28] K. Ebnabbasi, D. Busuioc, R. Birken, M. Wang, Taper design of vi-
440 valdi and co-planar tapered slot antenna (tsa) by chebyshev transformer,
441 IEEE Transactions on Antennas and Propagation 60 (2012) 2252–2259.
- 442 [29] B. Shuppert, Microstrip/slotline transitions: modeling and experimental
443 investigation, IEEE Transactions on Microwave Theory and Techniques
444 36 (1988) 1272–1282.

- ⁴⁴⁵ [30] H. Kim, R. Franklin-Drayton, Wire-bond free technique for right-angle
⁴⁴⁶ coplanar waveguide bend structures, IEEE Transactions on Microwave
⁴⁴⁷ Theory and Techniques 57 (2009) 442–448.